Adaptive Zero Padded CB-FMT for LTE Uplink Transmission in the High Mobility Scenario

Mauro Girotto
University of Udine
Udine 33100, Italy
Email: mauro.girotto@uniud.it

Andrea M. Tonello
University of Klagenfurt
Klagenfurt 9020, Austria
Email: andrea.tonello@aau.at

***Abstract*—LTE is the most recent standard for the mobile cellular communication. To achieve high speed communications, multi-carrier modulations have been adopted both for the downlink and the uplink. In the LTE downlink, OFDMA (the multi-user version of OFDM) has been chosen. The LTE uplink uses instead SC-FDMA modulation, an OFDM alternative. In this work, the use of CB-FMT, jointly with SC-FDMA, is analyzed in the high mobility scenario. Numerical results show that CB-FMT outperforms SC-FDMA in several cases. Thus, an adaptive implementation architecture that allows to flexibly choose the modulation scheme is proposed to maximize the achievable rate. Furthermore, for compliance with existing LTE parameters, frequency domain zero padded CB-FMT is proposed, and the problem of designing optimal capacity wise waveforms is considered.**

I. Introduction

Nowadays, high data rate communications are based on multi-carrier (MC) modulation. The most popular MC scheme is Orthogonal Frequency Division Multiplexing (OFDM) [1]. OFDM has been adopted in several wireless applications among which the downlink of the cellular LTE standard [2]. One of the major OFDM drawbacks is the high peak-to-average power ratio (PAPR) [3]. For this reason, in the LTE uplink scenario, Single Carrier FDMA (SC-FDMA) [4] has been adopted to reduce the cost of the power amplifiers, to increase the energy efficiency and to offer higher robustness in the uplink with mobile users.

In this paper, an alternative to SC-FDMA is considered for the LTE uplink. It is referred to as Cyclic Block Filtered Multitone Modulation (CB-FMT) [5]. This scheme is based on the idea of using a cylic filter bank (CFB) [6]. In CFB, the linear convolutions (involved in the filters) are replaced with circular convolutions. Thus, an efficient frequency domain (FD) implementation is possible. CB-FMT mimics the spirit of Filtered Multitone Modulation (FMT) [7], a filter bank modulation scheme designed to have high frequency confinement. The baseline version of CB-FMT adopts root-raised-cosine (RRC) prototype pulses. However, different pulse design methods can be adopted. In [8], orthogonality conditions and design algorithms have been presented.

Herein, a modified version of CB-FMT is introduced, namely Zero Padded CB-FMT (ZP-CB-FMT). This technique allows to add a band guard at the transmission band edges and it is used to allow the application in a system with LTE standard parameters. Furthermore, orthogonality aspects are investigated when zero padding is introduced in CB-FMT.

This paper is organized as follow. In Sec. II, the baseline concepts of CB-FMT are reported. Then, zero padded CB-FMT is introduced. In Sec. III, the main aspects involved in CB-FMT pulse design are reported. We show that a prototype pulse designed for a certain set of parameters can be reused for different sets of parameters. Finally, orthogonality aspects of ZP-CB-FMT are investigated. In Sec. IV, a brief overview on LTE uplink and associated parameters are reported. In Sec. V, a comparison between CB-FMT and SC-FDMA is performed in the high mobility scenario. Then, we show that an adaptive architecture can exploit the benefits of both schemes. Finally, in Sec. VI, the conclusions follow.

II. Cylic Block FMT Modulation

The CB-FMT transmitted signal is given by

$$x(nT) = \sum_{k=0}^{K-1} \sum_{\ell=0}^{L-1} a^{(k)}(\ell NT) g((n-\ell N)_M T) W_K^{-nk}, \quad (1)$$
$$n \in \{0, \cdots, M-1\},$$

where K, T and NT is the sub-channels number, the sampling period and the symbol period, respectively. The sub-channel symbols sequences are grouped in blocks of L data symbols and denoted as $a^{(k)}(\ell NT)$. The prototype pulse has a length of $M = LN$ samples. The operator $(\cdot)_M$ denotes the modulo operator, i.e., $(n + aM)_M = (n)_M$, $a \in \mathbb{Z}$. Thus, $g((n)_M T)$ represents the prototype pulse periodic repetition. The complex exponential function is defined as $W_K^{-nk} = e^{j2\pi nk/K}$.

At the receiver, the i-th received sub-sequence is given by

$$z^{(i)}(mNT) = \sum_{\ell=0}^{M-1} y(\ell T) W_K^{\ell i} h((mN-\ell)_M T), \quad (2)$$
$$i \in \{0, \ldots, K-1\}, \quad m \in \{0, \ldots, L-1\},$$

where $h((n)_M T)$ is the prototype pulse periodic repetition. In general, to maximize the signal-to-noise ratio (SNR) the transmitter and receiver pulses are matched, i.e., $h(nT) = g^*(-nT)$.

ISBN 978-0-9928626-7-1

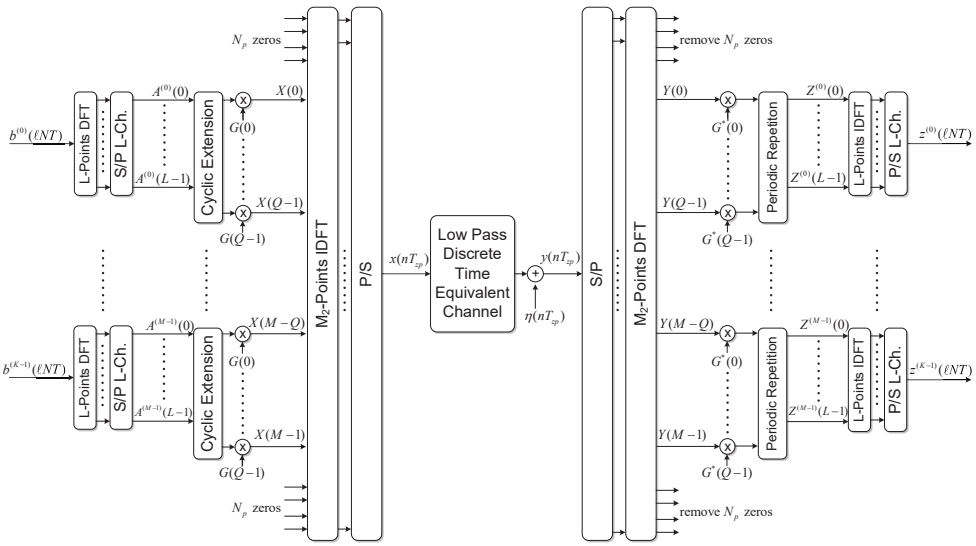

Fig. 1. Efficient frequency domain implementation of the zero padded CB-FMT transceiver.

A. Frequency Domain Zero Padded CB-FMT

When the prototype pulse is well confined into the sub-channel, i.e., the Discrete Fourier Transform (DFT) of the prototype pulse has only $Q = M/K$ non-zero coefficients, CB-FMT has a very efficient FD implementation. In fact, the M-point (inner) DFT of the transmitted signal in (1) yields

$$X(i) = A^{(k)}(i-kQ)G(i-kQ), \quad i \in \{kQ, \cdots, (k+1)Q-1\}, \quad k \in \{0, \cdots, K-1\}, \tag{3}$$

where $A^{(k)}(i)$ is the L-point (outer) DFT of k-th low rate sequence block $\left(a^{(k)}(\ell NT)\right)$ and $G(i)$ is the M-point DFT of the prototype pulse. Therefore, the transmitter comprises an inner IDFT and an K outer DFT (Fig. 1).

At the receiver, the L-point DFT of the signal (2) yields

$$Z^{(k)}(p) = \sum_{q=0}^{N-1} Y(p+qL+kQ)G^*(p+qL), \quad p \in \{0, \ldots, L-1\}, \quad k \in \{0, \ldots, K-1\}, \tag{4}$$

where $Y(p)$ is the M-point DFT of the received signal after the CP removal. Therefore, an inner M-point DFT, followed by FD equalization and K outer L-point IDFTs realize the receiver (Fig. 1).

We can note that the computational complexity is dominated by the inner M-point DFT/IDFT block. To exploit the FFT algorithm, M should be a power of 2. Since $M = LN = KQ$, all the system parameters (K, N, Q, L) should be power of two numbers. In this case, the normalized rate K/N is equal to 2^c, $c \in \{0, -1, -2, \ldots\}$. Excluding the critically sampled case ($K = N$), the maximum rate of the over-sampled case ($K < N$) becomes half of the maximum rate. Thus, when M is a power of 2, there does not exist an over-sampled configuration with normalized rate greater than 0.5.

To have M equal to a power of 2, without loss of generality, zero padding should be used. Exploiting the FD implementation, zero padding is simple to be obtained (see Fig. 1): the inner DFT is extended from M to M_2 points and the transmitted signal in (3) is placed into the central frequencies, i.e.,

$$X_{\text{zp}}(q) = \begin{cases} X(q-N_p) & \text{for } q-N_p \in \{0, \ldots, M-1\} \\ 0 & \text{otherwise} \end{cases}, \tag{5}$$

where $N_p = (M_2 - M)/2$. In (3), the coefficients spacing in FD is equal to $1/(MT)$ Hz. To keep the coefficients spacing constant after the zero padding, the sampling period must be adapted, so that $T_{\text{zp}} = T/\alpha$, where $\alpha = M_2/M$.

Zero padding can also be viewed as a time domain interpolation with a *sinc* shape filter. In detail, the M_2-point IDFT of the signal in (5) can be directly obtained from (1) as

$$x_{\text{zp}}(nT_{\text{zp}}) = \frac{e^{j\pi\left(\frac{\alpha-1}{\alpha}\right)n}}{\alpha M} \sum_{m=0}^{M-1} x(mT) g_i\left(n/\alpha - m\right), \tag{6}$$

where

$$g_i(a) = e^{j\pi\left(\frac{M-1}{M}\right)a} \frac{\sin(\pi a)}{\sin\left(\frac{\pi}{M}a\right)} \tag{7}$$

represents the periodic version of the sinc function.

At the receiver, the removal of the zero padding follows these steps: first, the M_2-point DFT of the received signal $y_{\text{zp}}(nT_{\text{zp}})$ is computed and denoted as $Y_{\text{zp}}(q)$. Then, only the middle frequency coefficients are considered to yield $Y(q)$, i.e.,

$$Y(q) = Y_{\text{zp}}(q+N_p), \quad q \in \{0, \ldots, M-1\}. \tag{8}$$

ISBN 978-0-9928626-7-1 © EURASIP 2017

In time domain, the zero padding removal is equivalent to a decimation. The signal $y(nT)$ can be directly obtained from $y_{\text{zp}}(nT_{\text{zp}})$ as

$$y(nT) = \frac{e^{-j\pi\left(\frac{\alpha-1}{\alpha}\right)n}}{\alpha M} \sum_{m=0}^{M_2-1} y_{\text{zp}}(mT_{\text{zp}}) g_i\left(n - m/\alpha\right), \quad (9)$$

The efficient ZP-CB-FMT transceiver is shown in Fig. 1.

B. Relation between CB-FMT and OFDM - SC-FDMA

OFDM and SC-FDMA modulations can be directly derived from the CB-FMT scheme with the appropriate parameters selection. Thus, CB-FMT can be seen as an adaptive architecture that is able to deploy SC-FDMA starting from the FD implementation of Fig. 1.

1) OFDM: this modulation can be obtained from CB-FMT when $L = 1$ and $K = N$. In this case, the prototype pulse shape and the outer L-point DFTs are not necessary. The transmitter in Fig. 1 is simply given by a K-point IDFT block (since $Q = 1$, $M = K$). In other words, OFDM can be seen as a CB-FMT scheme with a rectangular prototype pulse in time domain.

2) SC-FDMA: this modulation can be obtained when $K = N$ and the prototype pulse has a rectangular shape in FD, i.e., $G(i) = 1$ for $i \in \{0, \ldots, Q-1\}$ and 0 otherwise. Thus, the pulse shaping is transparent. Moreover, since $K = N$, the cyclic extension blocks in Fig. 1 are not necessary. The transmitter is simply given by a series of L-point DFT blocks (one for each sub-channel) that feed the outer M-point IDFT block. In other words, SC-FDMA can be seen as a CB-FMT scheme with a rectangular prototype pulse in FD.

III. Pulse Design

The CB-FMT system is designed to fulfill the orthogonality conditions. When these conditions are satisfied neither inter-channel interference (ICI) nor inter-symbol interference (ISI) will be exhibited at the receiver output.

Given a general CB-FMT system with a set of parameters (K, N, M), there exists an infinite number of prototype pulses that satisfy no-ISI and no-ICI conditions. For this reason an optimal pulse can be found under the goal of maximizing an objective function. In this work, the maximum achievable rate (capacity) is considered. This metric can be computed as

$$f\left(\mathbf{G}\right) = \frac{1}{(M+\mu)T} \sum_{k=0}^{K-1} \sum_{\ell=0}^{L-1} \log_2\left(1 + \text{SINR}^{(k)}(\ell, \mathbf{G})\right), \quad (10)$$

where $\mathbf{G}$ is the $M \times 1$ vector that contains the $G(i)$ coefficients, and $\text{SINR}^{(k)}(\ell, \mathbf{G})$ represents the signal-to-noise-plus interference of the ℓ-th data symbol of the block transmitted in the k-th sub-channel.

An important observation involves the critically sampled case when the pulse is well confined, i.e., in the SC-FDMA configuration. In this case, the only possible solution is the rectangular window. Thus, in this case, the optimization is not applicable.

More details are reported in [8].

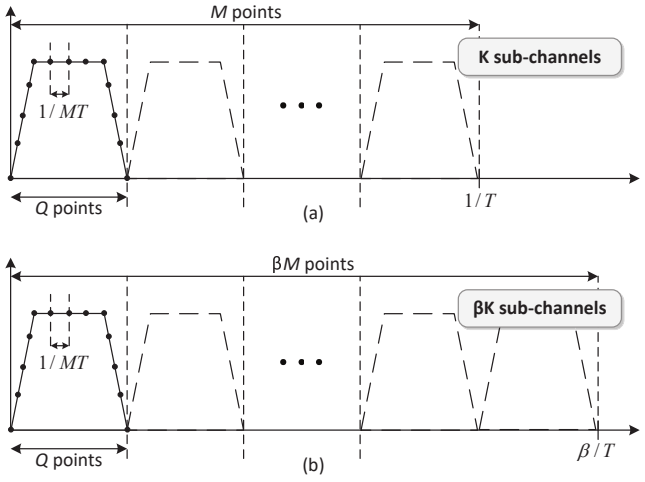

Fig. 2. Graphical representation of the parameters extension. On the top, the mother pulse designed for (K, N, M, T). On the bottom, the new orthogonal pulse valid for the set of parameters $(\beta K, \beta N, \beta M, T/\beta)$.

A. Parameters Extension

An important property of the frequency confined prototype pulses is their reuse under parameters variation. Given an orthogonal prototype pulse, designed for a set of parameters, it can be "reused" for a system where the parameters are scaled with a certain factor. The extended pulse, obtained from the mother pulse, satisfies the orthogonality conditions too [8].

This property has an important application in the LTE uplink. As shown in Sec. IV, LTE offers a set of SC-FDMA configurations that have different bandwidth occupancy. Given an LTE configuration, another configuration can be obtained scaling the parameters with a factor $\beta \in \mathbb{Q}$. Given a prototype pulse designed for the parameters set (K, N, M, T), it can be used for a CB-FMT system with parameters $(\beta K, \beta N, \beta M, T/\beta)$, $\{\beta K, \beta N, \beta M\} \in \mathbb{N}_0$. The extended prototype pulse in defined as

$$G_\beta(i) = \begin{cases} \sqrt{\beta} G(i) & \text{for } i \in [0, \ldots, Q-1] \\ 0 & \text{otherwise} \end{cases}, \quad (11)$$
$$i \in [0, \ldots, \beta M - 1].$$

The parameters extension is graphically represented in Fig. 2.

B. Orthogonality of ZP-CB-FMT and Equalization

To verify that the zero padding does not destroy the orthogonality, the system is modeled in matrix form. Without ZP, the received signal, after the M-point DFT block, is given by

$$\mathbf{Y} = \mathbf{F}_M \mathbf{H}_{\text{eq}} \mathbf{F}_M^H \mathbf{X}, \quad (12)$$

where $\mathbf{Y}$ and $\mathbf{X}$ are the $M \times 1$ vectors that gather the $Y(i)$ and $X(i)$ coefficients. $\mathbf{F}_M$ and $\mathbf{H}_{\text{eq}}$ are the M-point DFT matrix and the equivalent filter circulant matrix, respectively. The equivalent matrix takes into account the effects of the D/A-A/D converters filter and the transmission medium.

ISBN 978-0-9928626-7-1 © EURASIP 2017

When ZP is introduced, $\mathbf{Y}$ is given by

$$\mathbf{Y} = \mathbf{P}^T \mathbf{F}_{M_2} \mathbf{H}_{\text{eq}} \mathbf{F}_{M_2}^H \mathbf{P} \mathbf{X}, \tag{13}$$

where $\mathbf{P}$ is a $M_2 \times M$ matrix defined as

$$\mathbf{P} = \begin{bmatrix} \mathbf{0}_{N_p,M} \\ \mathbf{I}_M \\ \mathbf{0}_{N_p,M} \end{bmatrix}. \tag{14}$$

Denoting with $\mathbf{H}_2$ the matrix $\mathbf{F}_{M_2} \mathbf{H}_{\text{eq}} \mathbf{F}_{M_2}^H$, the matrix multiplication $\mathbf{H}_3 = \mathbf{P}^T \mathbf{H}_2 \mathbf{P}$ gives the $\mathbf{H}_2$ matrix with the first and last N_p rows/columns removed. The element at the p-th row and q-th column of $\mathbf{H}_3$ is given by

$$\{\mathbf{H}_3\}_{p,q} = \sum_{s=0}^{M_2-1} \sum_{n=0}^{M_2-1} h_s(nT_{\text{zp}}) W_{M_2}^{s(p+N_p)+n(q+N_p)}, \tag{15}$$

where $h_s(nT_{\text{zp}})$ are the equivalent filter coefficients. Three cases can be distinguished:

1) If the equivalent filter is ideal, namely a dirac delta, $\mathbf{H}_3$ is the identity matrix and the orthogonality is kept.
2) If the equivalent filter is time-invariant, $\mathbf{H}_3$ is a diagonal matrix. In this case, a 1-tap equalizer restores the orthogonality, i.e., $Y(q) = C_{\text{tinv}}(q)X(q)$, where $C_{\text{tinv}}(q)$ are the MMSE equalizer coefficients.
3) If the equivalent filter is time-variant, $\mathbf{H}_3$ is not a diagonal matrix. Assuming to deploy a simple 1-tap equalizer also for this situation, the orthogonality is not restored and some interference may remain. More details can be founded in [5], [8].

IV. LTE Uplink Overview

At the uplink, SC-FDMA modulation is adopted in the LTE standard. The number of sub-carriers that creates a SC-FDMA symbol is related to the channel bandwidth configuration adopted by the operator, from 1.4 to 20 MHz. LTE operates in several frequency bands that vary among the continents. The main LTE bands are are 800, 1800 and 2600 MHz.

In frequency division duplexing mode, the LTE transmission is partitioned (in time domain) in frames that have a duration of 10 ms. A frame is composed by 10 sub-frames and each sub-frame is divided in two slots of 0.5 ms. In normal CP configuration, used for small/medium cells, each slot contains 7 SC-FDMA symbols. The FD spacing, i.e., $1/(MT) = 1/(M_2 T_{\text{zp}})$, is constant and equal to 15 kHz. The M inputs of the M-point inner IDFT block are referred to as Resource Elements (REs). The smallest resource unit assigned to an user, namely the resource block (RB), comprises 12 REs (180 kHz). 12 REs is the size of the outer L-point DFT block of the SC-FDMA scheme. Exploiting the CB-FMT architecture (Fig. 1) for the realization of SC-FDMA, the parameters become $L = Q = 12$. The CP has a duration of 4.69 μs [9]. LTE supports scalable system bandwidths with the same frequency spacing and symbol duration. The available configurations are reported in Tab. I.

The E-UTRAN requirements [10] specify that LTE shall support mobility across the cellular network for different user speed levels. The communication is optimized for low mobility, below 15 km/h. In the speed range between 15 and 120 km/h the communication should be supported with high performance. The connectivity shall be maintained at speeds from 120 km/h to 350 km/h (or even up to 500 km/h depending on the frequency band). Given these high range of speeds, it becomes interesting to devise improved and robust modulation schemes.

TABLE I
LTE bandwidth configuration parameters expressed in terms of ZP-CB-FMT system.

Bandwidth (MHz)	K[a]	M	M_2	$1/T_{\text{zp}}$ (MHz)	β[b]
1.4	6	72	128	1.92	2/5
3	15	180	256	3.84	1
5	25	300	512	7.68	5/3
10	50	600	1024	15.36	10/3
15	75	900	1536	23.04	5
20	100	1200	2048	30.72	20/3

[a] Number of available Resource Blocks.
[b] Scaling factor w.r.t. the 3 MHz configuration.

V. Numerical Results

A. ZP-CB-FMT Parameters Selection and Pulse Design

To design the zero padded CB-FMT system, the SC-FDMA parameters reported in Tab. I are adopted. Thus, Q, K, M and M_2 follow the LTE standard. The remaining parameter is the interpolation factor N. The design is constrained by the relation $M = LN = KQ$. Since (Q, K, M) are defined, N must be a sub-multiple of M. For the LTE channel bandwidth between 3 and 20 MHz, we set $L = 10$ and $K/N = 5/6$. For the 1.4 MHz band, we set $L = 9$ and $K/N = 3/4$.

The algorithm reported in [8] is used to design the prototype pulse that maximizes the capacity. A time-variant and time-dispersive fading wireless channel with the Clarke's isotropic scattering model is assumed [11]. The normalized delay spread is equal to $\gamma = 3$ and the SNR is set equal to 40 dB. The pulse can be optimized w.r.t. a certain Doppler frequency. To limit the number of pulses, we have considered the 1.4 and 3 MHz bands and a maximum Doppler frequency of 1 kHz. For the others bands, the pulses are obtained from the mother pulse in the 3 MHz band configuration (see Sec. III-A).

B. Performances over Time-Variant Channels

To evaluate the performances of CB-FMT w.r.t. SC-FDMA in high mobility scenario, the maximum achievable rate is computed as a function of the Doppler frequency for every LTE bandwidth configuration. In Fig. 3 (left), the maximum achievable rate is shown for the 10 MHz bandwidth ($K = 50$, $M = 600$). CB-FMT outperforms SC-FDMA when the Doppler frequency is greater than 200 Hz, although not shown, the same behavior is found for all the LTE configurations with the exception of the 1.4 MHz bandwidth case. In this case, CB-FMT outperforms SC-FDMA when the Doppler frequency is greater than 600 Hz. The sub-optimal pulse is obtained with

ISBN 978-0-9928626-7-1 © EURASIP 2017

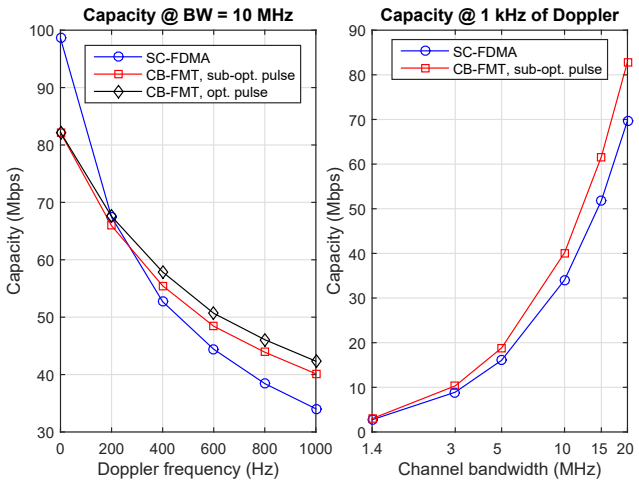

Fig. 3. On the left, the capacity as a function of the the Doppler frequency for the 10 MHz configuration. On the right, the capacity as a function of the LTE bandwidth for the maximum Doppler frequency (1 kHz).

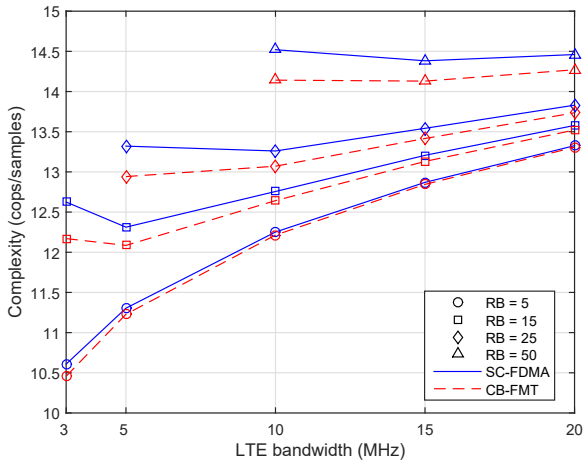

Fig. 4. Complexity of CB-FMT and SC-FDMA for different Resource Blocks allocation as a function of LTE bandwidth. The complexity is expressed in terms of complex operation per samples.

parameters extension described in Sec. III-A. The figure shows that the sub-optimal pulse offers a system capacity that is close to the optimal ones. Fig. 3 (right) shows the achievable rate as a function of the LTE bandwidth at the maximum Doppler frequency. In this case, CB-FMT outperforms SC-FMA.

C. Adaptive Architecture and Complexity

As shown, CB-FMT can outperform SC-FDMA in high mobility scenarios. Furthermore, it has been shown that a common implementation architecture can be used (Fig. 1). Therefore, optimal performance across a wide range of mobility situations can be obtained by adaptively using the two schemes, yet exploiting the same implementation structure. The complexity only slightly changes between the two modulations, as shown in Fig. 4. The complexity is expressed in terms of complex operations (cops) per sample at the transmitter when the FD implementation of Fig. 1 is used. Complexity is shown for different number of RBs allocated to the user and is evaluated as

$$C = N_{\mathrm{RB}} \frac{\lambda L \log_2 L + C_{\mathrm{sp}}}{M_2} + \lambda \log_2 M_2, \quad \left[\frac{\mathrm{cops}}{\mathrm{sample}}\right], \quad (16)$$

where N_{RB} is the RB number used and $\lambda = 1.2$. The block size L is equal to 10 for CB-FMT and 12 for SC-FDMA. C_{sp} represents the number of complex product involved in the sub-channel pulse shaping. In SC-FDMA, $C_{\mathrm{sp}} = 0$. In CB-FMT, $C_{\mathrm{sp}} = 4$ because 8 coefficients of the pulse are equal to 1 and, therefore, are transparent. Since CB-FMT has a lower rate w.r.t. SC-FDMA, the complexity is lower in all cases.

VI. Conclusions

The use of CB-FMT in LTE uplink has been addressed. The high mobility scenario has been considered and the achievable rate has been analyzed as a function of the Doppler frequency. For CB-FMT, the prototype pulse has been optimized to maximize the capacity at the Doppler frequency equal to 1 kHz. Numerical results show that CB-FMT outperforms SC-FDMA in several cases. Thus, an adaptive architecture can exploit the benefits of both schemes. The CB-FMT FD implementation can be used to switch between the two modulations. In detail, for low-medium speeds (Doppler frequency less than 200 Hz), SC-FDMA offers the greatest performance. For high speeds (Doppler frequency greater than 200 Hz), CB-FMT is superior due to the higher robustness offered by the well frequency confined sub-channels. CB-FMT offers also better PAPR characteristics than OFDM [5].

References

[1] J. A. C. Bingham, "Multicarrier Modulation for Data Transmission, an Idea whose Time Has Come," *IEEE Communication Magazine*, vol. 31, pp. 5–14, May 1990.

[2] D. Astely, E. Dahlman, A. Furuskar, Y. Jading, M. Lindstrom, and S. Parkvall, "LTE: The Evolution of Mobile Broadband," *IEEE Communications Magazine*, vol. 47, no. 4, pp. 44–51, April 2009.

[3] P. W. J. Van Eetvelt, S. J. Shepherd, and S. K. Barton, "The Distribution of Peak Factor in QPSK Multi-Carrier Modulation," *Wireless Personal Communications*, vol. 2, no. 1, pp. 87–96, 1995.

[4] H. G. Myung, J. Lim, and D. J. Goodman, "Single Carrier FDMA for Uplink Wireless Transmission," *IEEE Vehicular Technology Magazine*, vol. 1, no. 3, pp. 30–38, Sept 2006.

[5] A. M. Tonello and M. Girotto, "Cyclic Block Filtered Multitone Modulation," *EURASIP Journal on Advances in Signal Processing*, vol. 2014, no. 1, p. 109, 2014.

[6] P. P. Vaidyanathan and A. Kirac, "Theory of Cyclic Filter Banks," in *IEEE Int. Conf. on Acoustics, Speech, and Signal Processing (ICASSP-97)*, vol. 3, Apr 1997, pp. 2449–2452.

[7] G. Cherubini, E. Eleftheriou, and S. Olcer, "Filtered Multitone Modulation for Very High-Speed Digital Subscriber Lines," *IEEE JASC*, vol. 20, no. 5, pp. 1016–1028, Jun 2002.

[8] M. Girotto and A. Tonello, "Orthogonal design of cyclic block filtered multitone modulation," *IEEE Trans. on Communications*, vol. 64, no. 11, Nov 2016.

[9] S. Sesia, I. Toufik, and M. Baker, *LTE - The UMTS Long Term Evolution: From Theory to Practice*. Wiley, 2011.

[10] "Universal Mobile Telecommunications System (UMTS); LTE; Requirements for Evolved UTRA (E-UTRA) and Evolved UTRAN (E-UTRAN)," TR 125 913, ETSI, 2009.

[11] G. L. Stuber, *Principles of Mobile Communication*, 2nd ed. Kluwer Academic Publishers, 1996.

ISBN 978-0-9928626-7-1 © EURASIP 2017